IEEE Photonics Journal
An IEEE Photonics Society Publication

Open Access

GaN Membrane With Nano-Grooves for Single-Band Coupling in the Entire Visible Wavelength Range

Volume 10, Number 2, April 2018

Qifa Liu
Cheng Wang
Wenlei Yang
Huihui Wang
Rongqing Xu

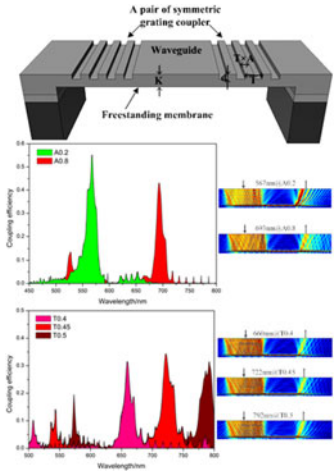

DOI: 10.1109/JPHOT.2018.2815016
1943-0655 © 2018 IEEE

IEEE photonics SOCIETY

IEEE

GaN Membrane With Nano-Grooves for Single-Band Coupling in the Entire Visible Wavelength Range

Qifa Liu,[1] **Cheng Wang**,[1] **Wenlei Yang**,[2] **Huihui Wang**,[1] **and Rongqing Xu**[3]

[1]College of Telecommunication and Information Engineering, Nanjing University of Posts and Telecommunications, Nanjing 210003, China
[2]Key Laboratory of In-fiber Integrated Optics of Ministry of Education, College of Science, Harbin Engineering University, Harbin 150001, China
[3]College of Electronic and Optical Engineering & College of Microelectronics, Nanjing University of Posts and Telecommunications, Nanjing 210023, China

DOI:10.1109/JPHOT.2018.2815016

Manuscript received February 7, 2018; revised February 26, 2018; accepted March 7, 2018. Date of publication March 12, 2018; date of current version March 29, 2018. This work was supported in part by the Natural Science Foundation of Jiangsu Province of China under Grants BK20150861 and BK20151508, in part by the National Natural Science Foundation of China under Grant 11704086, and in part by the Research Projects of Nanjing University of Posts and Telecommunications under Grant NY214036. *(Qifa Liu and Cheng Wang contributed equally to this work.)* Corresponding author: Rongqing Xu (e-mail: xurq@njupt.edu.cn).

Abstract: Nano-groove arrays incorporated into a freestanding GaN membrane are proposed for coupling with visible light. The coupling of transverse electric mode light over the entire visible wavelength region into and out of the planar membrane is thoroughly investigated herein by performing a finite element method analysis. Coupling can be regulated by device parameters such as groove depth, membrane thickness, grating period, and duty cycle. Single-band coupling featuring tunable coupling bands can be realized, with the peak dual coupling efficiency reaching 0.55. This study paves the way for realizing planar photonics devices at specific single wavelengths. The proposed device is a suitable candidate for use in optical filters, de-multiplexers, planar photonic sensors, and other devices.

Index Terms: GaN membrane, nano-grooves, single-band tunable coupling, visible wavelength, FEM.

1. Introduction

Gallium nitride (GaN) is an active material representative of III–V compounds. It is the basic material of the most popular blue light light-emitting diodes (LEDs) and laser diodes (LDs). GaN is also a promising material for other optical applications, due to its wide transparent wavelength range, high refractive index, outstanding mechanical and chemical properties, and chemical inertness [1]–[3]. It can be made into high contrast grating (HCG) reflectors. By using the GaN-based HCG as reflector for multiple quantum wells (MQWs), Wu *et al.* designed and fabricated surface-emitting lasers [4]. Lee *et al.* developed a one-dimensional sub-wavelength grating structure on a GaN surface that behaves as a reflector for transverse electric polarized light in the blue wavelength range [5]. The etched gratings on GaN act as mirrors in GaN-based LDs and promote external quantum efficiency for LEDs [6].

Another important application of GaN is in planar photonics, where it can be employed in a variety of fields and exhibits outstanding properties. GaN-based planar photonic devices have been widely reported because of their high coupling efficiency when incorporated into waveguides [7]. Trivino *et al.* [8] reported GaN self-supported planar structures consisting of free-standing waveguides coupled to photonic crystal waveguides. Zhang *et al.* [9] discussed the fabrication of rib GaN waveguides on a sapphire substrate using inductively coupled plasma etching. Hui *et al.* [10] designed, fabricated, and characterized single-mode ridged optical waveguide devices using GaN/AlGaN hetero-structures for operation at 1550 nm wavelength.

Nonetheless, studies regarding GaN planar photonics in the visible region have not been a focus compared to those of the near-infrared band. Nevertheless, visible band photonics is promising for various applications such as signal processing [11], communication [12] and sensing [13], [14]. The excellent properties of GaN also make it a suitable candidate for planar photonics devices in the visible region. Dylewicz *et al.* [15] achieved grating-assisted coupling into/from GaN planar waveguides on sapphire at 632.8 nm. Suspended GaN-based nanostructure visible wavelength planar photonics devices were obtained by exciting an InGaN/GaN MQWs active layer while some of the emitted light was confined inside epitaxial films [16].

To the best of our knowledge, no previous studies have considered the entire visible region in the production of single-band photonics devices and to de-multiplex white input light. Previously reported devices are also not capable of being used as optical filters and do not have tunable features. Previously, we reported a free-standing GaN membrane grating coupler and waveguide at visible wavelengths [17]. When white light was irradiated, some wavelength bands exhibited high coupling efficiency. The device was fabricated using a double-sided fabrication process on a GaN-Si platform. By employing the same technique, freestanding GaN devices have been reported in applications featuring excited light extraction promotion, reflectance, and emitter modulation [18]–[20]. This platform and fabrication method is capable of tuning nano-parameters, particularly the GaN thickness, which is crucial to satisfying the single-band condition. Therefore, GaN photonics with more outstanding features at visible wavelengths can be developed using this strategy.

In this study, the freestanding membrane thickness and grating groove parameters controlling visible light coupling were investigated by finite element method (FEM) simulation. The grating coupler is an excellent solution for out-of-plane coupling and an effective way to realize planar photonics devices [21]–[23]. It is suitable for use in applications such as fiber-chip-fiber coupling [24]–[26], light sources and planar photonic integration [27], and wafer scale testing and sensing [28], [29]. In this study, groove arrays were fabricated by single-step etching as the grating couplers. The tunable groove parameters and waveguide thickness are favorable for realizing single-band coupling in the entire visible band, making this device promising for realizing planar photonics devices at specific wavelengths for use in optical filters, de-multiplexers, and other devices.

2. Prototype Structure and Modeling

Fig. 1 shows a prototype of the GaN membrane with nano-grooves as a pair of uniform gratings in a freestanding GaN membrane. The device structure, as developed in our previous study [17], is defined by the following crucial parameters: the membrane thickness K, groove depth d, uniform groove period T, duty cycle A and grating bar width $T \times A$. Because of the two-dimensional simulation used in this study, the structure is a slab waveguide, and the membrane width was not considered. Since the silicon-based platform is suitable for preparing the freestanding micro-nano device structure, and because the silicon-based GaN wafer is commercially available, the proposed structure can be successfully fabricated by starting with a GaN/AlGaN/AlN/Si platform. The AlGaN/AlN intermediate layer is a buffer layer that alleviates crystal lattice mismatch between GaN and Si.

The fabrication process, as shown in Fig. 1, uses mature silicon bulk micromachining combined with traditional micro-nano fabrication. First, the uniform groove array was defined by electron beam lithography (EBL) and etched by inductively coupled plasma reactive ion etching (ICP-RIE). Then, after backside alignment photolithography, the silicon substrate was removed by deep reactive

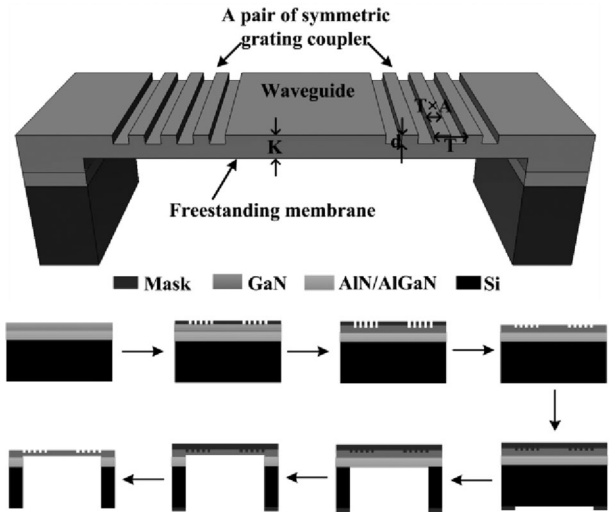

Fig. 1. Schematic illustration of the prototype structure and fabrication process. *T*: groove period, *A*: duty cycle, *d*: groove depth, *K*: membrane thickness.

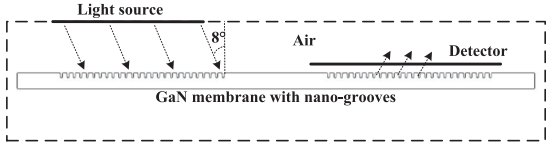

Fig. 2. Simulation model for the GaN grooves coupling.

ion etching (DRIE) to produce a freestanding III-V compound membrane. Afterwards, continuous etching of the AlN, AlGaN and GaN layers was performed using the same etching process as in the GaN grating groove etching. Finally, after releasing the mask, a pure GaN membrane with two groove array regions was obtained.

The platform and the fabrication method produce unique freestanding planar structures featuring controllable membrane waveguide thickness, groove depth and grating teeth width, which all influence the light coupling.

To investigate the influence of nano-parameters on the coupling performance and to optimize the coupling band and coupling efficiency, the finite element method (FEM) simulation was performed. The influence of the groove depth, membrane thickness, groove period and duty cycle on coupling was systematically analyzed. We used these tunable parameters to investigate and optimize the single-band coupling in the entire visible region. Thus, this investigation can help inform the design of an optical filter, a de-multiplexer and single-band planar photonics devices at visible wavelengths.

The 2D FEM simulation model based on COMSOL Multiphysics is shown in Fig. 2. There are two grating regions on the GaN membrane to diffract light into and out of the membrane waveguide separately. The light source was defined in the model boundary with a length of 10 μm and was considered to be a plane wave. We defined the electric field only along the direction parallel to the groove lines for every wavelength. The incident angle was constant at 8° to break the diffraction symmetry, eliminate reflection and reduce return loss [30], [31]. The detector was placed above the out-coupling grating region. It is always 2 μm longer than the length of the grating region, which varies with grating period, and was positioned close to the grating at a distance of 400 nm. The detector is just a position to make calculations, which has no effect on light. Considering the out-coupling profile may not regular and features divergent in the propagation direction, the detector design in the model guarantees the accurate detection of all the out-coupling energy, to obtain theoretical results. Eliminating the influence of collection loss and calculating out the ideal

theoretical values is important for systematically investigation and design of device parameters. The coupling of transverse electric mode (TE) waves at 400–800 nm was investigated, and the linear gratings were found to be strongly polarization-dependent. TE wave is an incident beam with E-field polarization parallel to the groove lines. The grating has 26 periods, which guarantees all the light source energy irradiate on the gratings region. Besides, the illuminated position is exactly fixed as the same in each calculation. All boundaries were defined as the scattering boundary condition which absorbs all the incident waves to imitate boundless space. The model is meshed by free triangulation with a maximum and minimum element size of 150 and 4 nm, respectively, with a 1.2 times growth rate. The refractive index of the surrounding air was set as 1, whereas that of GaN was defined as a function of the wavelength $\lambda = 0.4$–$0.8\,\mu$m.

$$n_{GaN} = \left(3.6 + \frac{1.75 \times \lambda^2}{\lambda^2 - 0.256^2} + \frac{4.1 \times \lambda^2}{\lambda^2 - 17.86^2}\right)^{0.5} \tag{1}$$

The coupling can be roughly described by the Bragg condition. When the diffraction resonant modes in the grating region match the waveguide mode, known as the phase-matching condition (2), coupling occurs.

$$\lambda / T = n_{eff} - n_0 \sin\theta \tag{2}$$

where T is the grating period, n_{eff} is the effective index of the grating region, λ is the free-space wavelength, n_o is the refractive index of the surrounding air, and θ is the incident angle of the light. When the component of the $+1$ order diffraction vector along the propagation direction of the guided mode matches that of the mth order waveguide mode, which is described by the phase-matching condition, the propagation of the mth order waveguide mode can be excited in the waveguide.

Considering the very short waveguide length (only several micrometers long) between the two grating regions in the simulation model, the transmission loss in the membrane waveguide was assumed to be zero. After coupling in and out of the membrane waveguide, the dual coupling efficiency can be calculated using the following equation:

$$\eta_d = E_{out} / E_{in} \tag{3}$$

where E_{in} and E_{out} represent the total field energy emitted from the light source and out onto the detector, respectively. Although the energy distribution of the light source and the detector is not uniform, the coupling efficiency can be calculated by the line integration value of time-averaged field energy of the detector divided by that of the light source. Thus, the calculated efficiency reflects the summation of the out-energy of the detector divided by the summation of the in-energy of the light source at every wavelength. The calculated coupling efficiency is theoretical value, which not considering the actual loss when using specific detector to collect light.

The in-coupling and out-coupling for the two groove regions are symmetrical and have similar coupling efficiency. Thus, the single coupling efficiency by one groove region can be calculated by the following equation:

$$\eta_s = \sqrt{E_{out} / E_{in}} \tag{4}$$

The data used in the following discussion were calculated using (3), unless specified otherwise.

3. Discussion on Nano Parameters Depending Coupling

3.1 Influence of Groove Depth and Membrane Thickness

Coupling occurs mainly due to light diffraction in the nano-grooves, and is strongly influenced by the depth of the etched-groove [32], [33]. To investigate the effect of the groove depth d, the parameters were defined as: $T = 0.5\,\mu$m, $A = 0.7$, $K = 1.77\,\mu$m, as previously determined [17]. Based on the previously prepared device, the design of the device in this study is feasible and practical. Fig. 3 demonstrates the coupling efficiency contour map with varying groove depths and wavelengths. The results show that, there are many coupling bands at each etched depth investigated. The

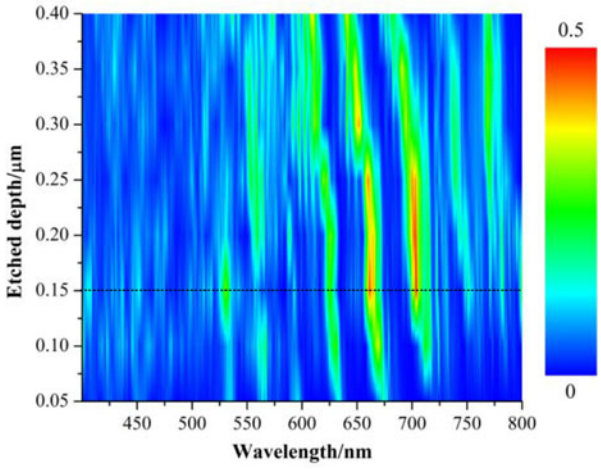

Fig. 3. Coupling efficiency contour plot as a function of wavelengths and groove etched depth.

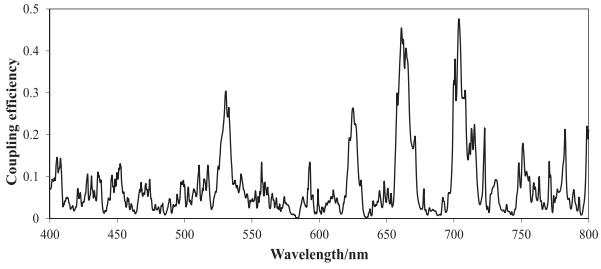

Fig. 4. Coupling efficiency plot as a function of wavelength at an etched depth of 0.15 μm.

etched depth has a limited influence on the coupling wavelength, because the coupling bands do not have an apparent movement; however, the depth has a significant influence on the coupling efficiency. The optimized etched depth was determined to be 0.15 μm by only considering the coupling efficiency as an indicator. The dashed line in Fig. 3 indicates the coupling efficiency plot as a function of the wavelength at this optimized etched depth, shown in Fig. 4. Two high coupling bands can be observed and the maximum coupling efficiency reached 0.47 at 708 nm and 0.45 at 660 nm.

The planar waveguide thickness is an important parameter for the confined light mode [19], [34]. In our simulation model, the GaN membrane waveguide belongs to a three layer symmetric slab waveguide with air as its cladding. The guided modes can be calculated as follows:

$$m = int\left[\frac{2 \times K \times \left(n_{GaN}^2 - n_{air}^2\right)^{0.5}}{\lambda}\right] \tag{5}$$

where m is the number of supported waveguide modes, K is the waveguide thickness, λ is the wavelength, n_{air} is 1, and n_{GaN} can be obtained from (1).

The proposed planar photonics devices in this study are capable of achieving various membrane waveguide thickness due to the wafer platform and fabrication process. The dual coupling efficiency for different waveguide thicknesses from 0.2 to 2 μm was investigated through simulations, while the grating period T was set as 0.5 μm, the duty cycle A was 0.7, and the etched depth d was set to be 0.15 μm from the optimization results. From (5), the membrane with a 2 μm thickness is a multi-mode waveguide in the entire visible range. The membrane with a 0.2 μm thickness was characterized as multi-mode at shorter wavelengths and single-mode at longer wavelengths. Fig. 5 shows the coupling efficiency and wavelength band variations as a function of membrane thickness. According to the contour map, with thicker films, increased coupling is observed. This is because

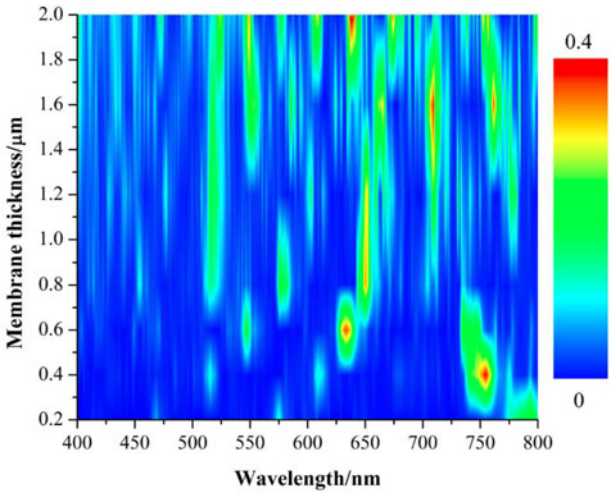

Fig. 5. Coupling efficiency contour plot as a function of wavelength and membrane thickness.

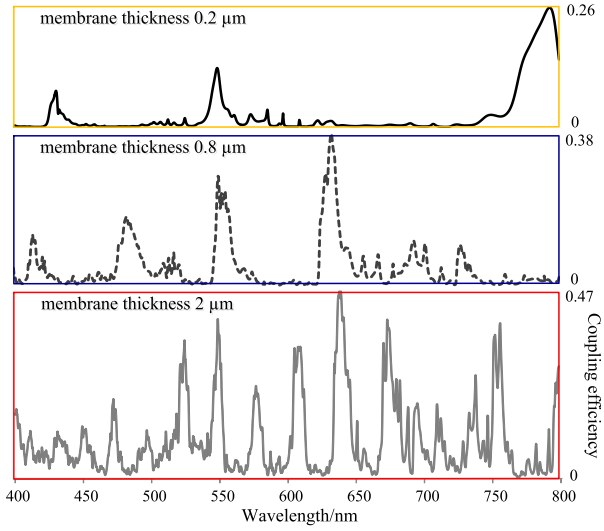

Fig. 6. Coupling efficiency plot as a function of wavelength at membrane thicknesses of 0.2, 0.8 and 2 μm.

thicker membrane result in more waveguide modes, and the multi-order optical waveguide mode can match the phase matching condition with a certain order of diffraction of multiple wavelengths. It can be deduced that single-band coupling could be realized via controlling suitable GaN film thickness. When the thickness is less than 0.4 μm, only one high-efficiency coupling band exists. Fig. 6 shows the coupling plot over the entire visible wavelength region at membrane thicknesses of 0.2, 0.8 and 2 μm, demonstrating the phenomenon more clearly. Thinner membranes support fewer modes and result in greater intervals between coupling bands. Thus, by regulating other parameters, single-band coupling at different wavelengths within the visible region can be achieved.

3.2 Groove Period and Duty Cycle Regulated Single-Band Coupling

Based on the above results, the nano-parameters were fixed at $d = 0.15$ μm, $K = 0.2$ μm, $A = 0.7$ to investigate the groove period influence on the coupling wavelength. The simulated result shown in Fig. 7 indicates that the coupling wavelength varies linearly with the period. The coupling wavelength

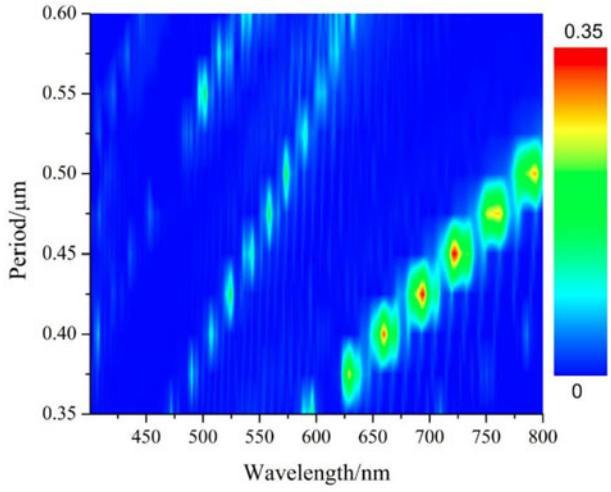

Fig. 7. Coupling efficiency contour plot as a function of wavelength and groove period.

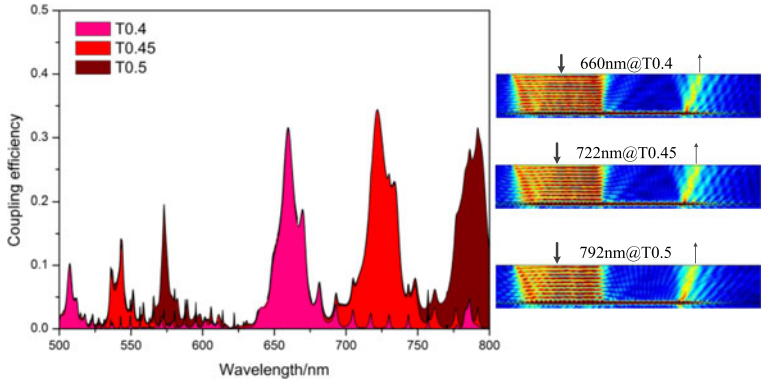

Fig. 8. Coupling efficiency plot as a function of wavelength and electric field distribution at the peak coupling wavelength when the groove period is 0.4, 0.45 and 0.5 μm respectively.

experiences an obvious red shift as the groove period increases from 0.35 to 0.6 μm. This can be explained by the phase-matching condition (2), which exhibits the bigger T the bigger λ. Every period has only one or two high-efficiency coupling bands in the entire visible wavelength range because the film is very thin. In addition, higher coupling efficiency occurs at periods of 0.4, 0.45 and 0.5 μm. Coupling efficiency plots as a function of wavelength are shown in Fig. 8. The filling color indicates to some extent the color of the out-coupling wavelength band with the highest coupling efficiency. The central wavelength (CWL) for coupling at $T = 0.4,\ 0.45$ and 0.5 μm is 660, 722 and 792 nm, respectively. The light field distributions at these peak coupling wavelengths are inset in Fig. 8 and the arrows indicate the direction of the light.

The 3 dB passband bandwidth ($BW_{3\,dB}$) can be calculated from $BW_{3\,dB} = W_2 - W_1$, where W_1 and W_2 are the wavelengths where the coupling efficiency drops 3 dB, by using the coupling efficiency at the CWL as the benchmark. The $BW_{3\,dB}$ of $T0.4$, $T0.45$ and $T0.5$ are as follows:

$$BW_{3\,dB}(T0.4) = 671\,\text{nm} - 653\,\text{nm} = 18\,\text{nm}$$
$$BW_{3\,dB}(T0.45) = 736\,\text{nm} - 715\,\text{nm} = 21\,\text{nm}$$
$$BW_{3\,dB}(T0.5) = 799\,\text{nm} - 776\,\text{nm} = 23\,\text{nm}$$

In addition to the peak coupling wavelength, another coupling band at each period was observed. In accordance with the peak wavelengths, three small coupling band wavelengths increased with the period. To evaluate the filtering performance of the device, the extinction ratio was introduced

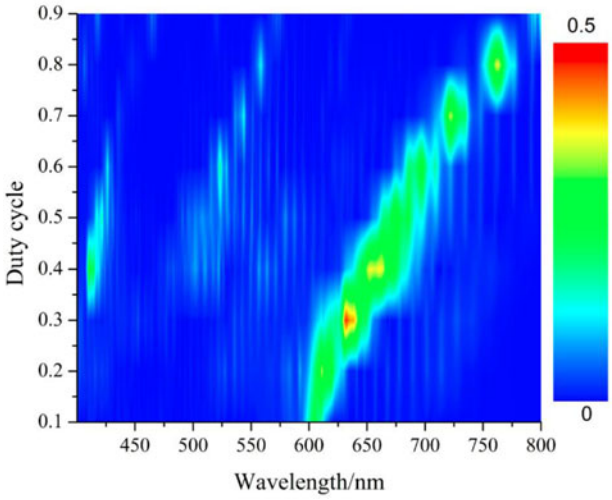

Fig. 9. Coupling efficiency contour plot as a function of wavelength and duty cycle.

and defined as $EXT = 10lg(Pc/Po)(dB)$, where Pc is the coupling efficiency of the coupling band and Po denotes the background maximum coupling efficiency over the entire wavelength region. The defined EXT can reflect the influence of other bands on the coupling band. Larger values of EXT indicate better filtering performance. The calculated EXT values of $T0.4$, $T0.45$ and $T0.5$ are listed below:

$$\mathrm{EXT}(T0.4) = 10\mathrm{lg}(0.31/0.1) = 4.9\,\mathrm{dB}$$
$$\mathrm{EXT}(T0.45) = 10\mathrm{lg}(0.34/0.13) = 4.2\,\mathrm{dB}$$
$$\mathrm{EXT}(T0.5) = 10\mathrm{lg}(0.29/0.17) = 2.3\,\mathrm{dB}$$

The duty cycle is another crucial parameter that regulates coupling. By combining period and duty cycle regulation, clear single-band coupling can be achieved. According to the results of the period investigation, a duty cycle from 0.1 to 0.9 was studied by fixing the period at 0.4 and 0.45 μm. Fig. 9 shows the influence of the duty cycle on the coupling when the period is 0.45 μm. The coupling wavelength increases gradually with increasing duty cycle; a similar trend was observed at a period of 0.4 μm. The physics behind the effect of the duty cycle on the coupling wavelength is related to changes in the effective index. Although the period was fixed, alteration of duty cycle changed the effective index of the grating region. The effective index also influences the coupling wavelength from the phase-matching condition of (2).

The coupling efficiency plot at $A = 0.2$ and 0.8 with a 0.45 μm period is shown in Fig. 10. The insets exhibit the light field distribution at the peak coupling wavelength with a CWL of 610 nm@$A0.2$ and 762 nm@$A0.8$.

The $\mathrm{BW}_{3\,\mathrm{dB}}$ values of $A0.2$ and $A0.8$ are as follows:

$$\mathrm{BW}_{3\,\mathrm{dB}}(A\,0.2) = 622\,\mathrm{nm} - 603\,\mathrm{nm} = 19\,\mathrm{nm}$$
$$\mathrm{BW}_{3\,\mathrm{dB}}(A\,0.8) = 769\,\mathrm{nm} - 754\,\mathrm{nm} = 15\,\mathrm{nm}$$

Fig. 11 shows the coupling efficiency plot at $A = 0.2$ and 0.8 with a 0.4 μm period and the corresponding light field distribution at the peak coupling wavelength. The CWL is 567 nm@$A0.2$ and 693 nm@$A0.8$.

The $\mathrm{BW}_{3\,\mathrm{dB}}$ values of $A0.2$ and $A0.8$ are calculated as follows:

$$\mathrm{BW}_{3\,\mathrm{dB}}(A\,0.2) = 576\,\mathrm{nm} - 557\,\mathrm{nm} = 19\,\mathrm{nm}$$
$$\mathrm{BW}_{3\,\mathrm{dB}}(A\,0.8) = 700\,\mathrm{nm} - 687\,\mathrm{nm} = 13\,\mathrm{nm}$$

From Figs. 10 and 11, it is clear that the device shows single-band coupling properties when $A = 0.2$ at different coupling CWLs owing to the groove period regulation. Although there is another

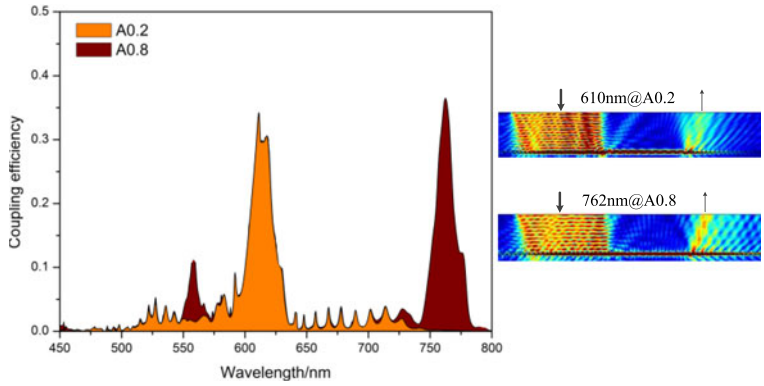

Fig. 10. Coupling efficiency plot as a function of wavelength and electric field distribution at the peak coupling wavelength when the duty cycle is 0.2 and 0.8, with a 0.45 μm period.

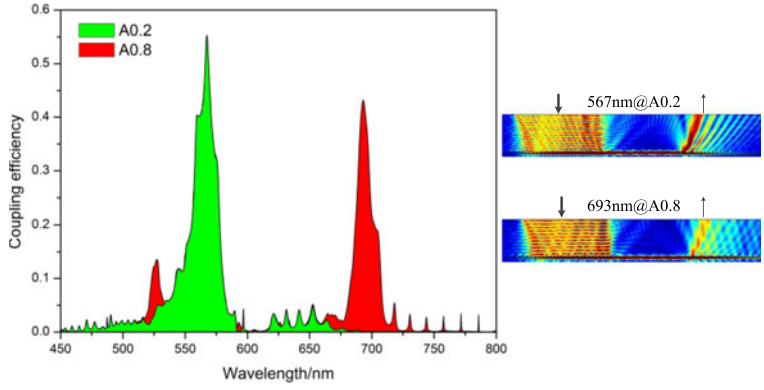

Fig. 11. Coupling efficiency plot as a function of wavelength and the electric field distribution at the peak coupling wavelength when the duty cycle is 0.2 and 0.8, with a 0.4 μm period.

coupling band when $A = 0.8$, a thinner membrane can be produced to eliminate the other band and to observe single-band coupling. From the electric field distribution in Figs. 10 and 11, weakened out-coupling field along the grating region can be observed. It is because the output beam of the uniform gratings has an exponentially decaying function along the direction of propagation.

The peak coupling efficiency shown in Fig. 11 is $\eta_d = 0.55$. When considering a single region grating coupling, a higher efficiency $\eta_s = 0.74$ was obtained according to (4). However, with regards to the optical filtering effect, dual coupling enhances the extinction ratio EXT compared to single coupling.

It should be noted that multiple resonance peaks are clearly observed in the coupling plot, which can be attributed to the Fabry-Perot (F-P) resonant effect caused by the simulation model. Because the simulation was performed by FEM, the membrane in the model has a specific length, which forms a resonant cavity. The F-P effect also results from the high refractive index contrasts at the GaN/air interfaces. Equation (6) describes the relationship between the waveguide length L, the effective refractive index of the waveguide mode at the peak wavelength $n_{(\lambda)}$, the peak wavelength λ, and the peak numbers i which counts from short wavelength to long wavelength [35]. From the equation, longer waveguides results in an increased number of resonance peaks. Besides, the change in the period or duty cycle of the gratings will affect $n_{(\lambda)}$, thus affecting the resonant wavelengths. The F-P resonance enhances the electromagnetic field intensity at the resonant wavelength.

$$i/L = -2n_{(\lambda)}/\lambda \tag{6}$$

The results presented herein indicate that the coupling wavelength is mainly determined by the grating period and duty cycle. The number of the coupling bands is mainly determined by the

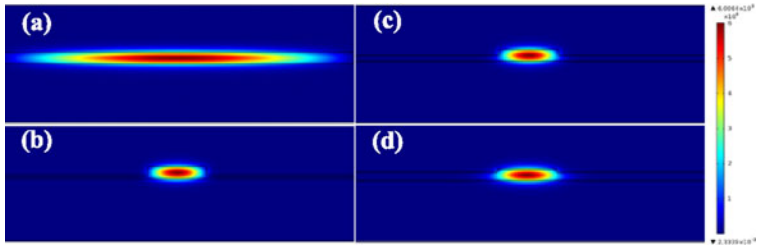

Fig. 12. Electric field mode distribution at wavelength 600 nm in membrane without rib (a), with 1 μm rib width while with 150nm etched depth (b), 100 nm etched depth (c), 50nm etched depth (d).

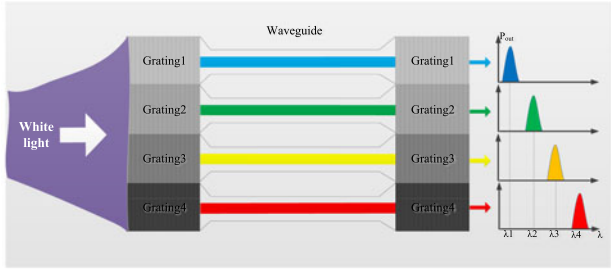

Fig. 13. Schematic of the device application.

membrane thickness. The coupling efficiency has a strong relationship with all parameters including the groove depth, membrane thickness, groove period, duty cycle and wavelengths. Single band coupling regulated in the whole visible range can be realized through the composite controlling of period *T* and duty cycle *A*. In order to guarantee high coupling efficiency while regulating coupling band, only *T0.45* and *T0.4* was focused, for they were previously optimized by coupling efficiency. Theoretically, any value of *T* and *A* can be selected to realize single band regulating at various wavelengths.

Aside from coupling loss, the transmission loss is another important prerequisite for actual device. The single-step patterning process is to realize gratings and rib waveguide in single etching step. Waveguide rib reduces the overlap between the optical mode and the waveguide sidewalls, thus the propagation loss can be effectively reduced. We designed 1 μm width rib structure for the above planar device, which with 150 nm etched depth and 200 nm waveguide thickness. Fig. 12(a) and (b) exhibits the mode profile at 600 nm wavelength in membrane without rib and with rib, respectively. More constricted mode is observed when membrane waveguide has the rib, and the constrained mode profile represents low propagation loss. Ribs with 100 nm and 50 nm etched depth were also investigated. The simulated results are shown in Fig. 12(c) and (d). It can be deduced from Fig. 12 that, rib with bigger depths produce slightly more constrained mode profile, which means a little smaller leakage in the direction parallel to the gratings.

There also exists lateral leakage on grating regions in the direction parallel to the grooves for the actual device. The grating bars have certain length, that cause interface with different effective refractive index between grooves region and non-grooves region. The leakage loss mainly occurred on this interface. The loss also varied with the difference of effective refractive index which tuned by grating parameters such as duty cycle. However, the loss is very limited due to the limited grating region length in the direction perpendicular to the grating and the orthogonal diffraction direction raised by gratings. Especially in this investigation, the gratings in the two-dimensional simulation model devotes to ideal gratings, which have infinite groove length in the direction parallel to the grooves. So there is no loss caused by lateral leakage in grating region.

In conclusion, the tunable characteristics undoubtedly endow outstanding properties of this novel device, which is a candidate for realizing planar photonics at specific wavelengths and for use as optical filters and de-multiplexers to extract particular wavelengths. Fig. 13 shows an example

scenario for the related device applications. The light is applied on the groove arrays with different parameters, and after experiencing dual coupling, light with different wavelengths/colors are separated.

4. Conclusion

We investigated the out-of-plane coupling of the TE mode over the entire visible region into and out of the GaN membrane waveguide by nano-groove diffraction. Based on the FEM simulation results, single-band coupling can be realized, and the coupling wavelength and efficiency are regulated by the nano-parameters of the device. The device can be used to implement planar photonics of particularly visible wavelength bands, and has the potential for incorporation into devices for applications such as optical filters, de-multiplexers and sensors.

References

[1] A. Rosenberg *et al.*, "Guided resonances in asymmetrical GaN photonic crystal slabs observed in the visible spectrum," *Opt. Exp.*, vol. 13, no. 17, pp. 6564–6571, 2005.
[2] C. Meier *et al.*, "Visible resonant modes in GaN-based photonic crystal membrane cavities," *Appl. Phys. Lett.*, vol. 88, no. 3, 2006, Art. no. 031111.
[3] Z. Yang *et al.*, "Mechanical characterization of suspended GaN microstructures fabricated by GaN-on-patterned-silicon technique," *Appl. Phys. Lett.*, vol. 88, no. 4, 2006, Art. no. 041913.
[4] T.-T. Wu, S.-H. Wu, T.-C. Lu, and S.-C. Wang, "GaN-based high contrast grating surface-emitting lasers," *Appl. Phys. Lett.*, vol. 102, no. 8, 2013, Art. no. 081111.
[5] J. Lee, S. Ahn, H. Chan, J. Kim, Y. Park, and H. Jeon, "Polarization-dependent GaN surface grating reflector for short wavelength applications," *Opt. Exp.*, vol. 17, no. 25, 2009, Art. no. 22535.
[6] R. Dylewicz *et al.*, "Low-dimensional waveguide grating fabrication in GaN with use of SiCl4/Cl2/Ar-based inductively coupled plasma dry etching," *J. Electron Mater.*, vol. 38, no. 5, pp. 635–639, 2009.
[7] X. Xing, X. Deng, and B. Li, "Analysis of GaN-based single-mode rib waveguide with large cross section," *J. Microlith. Microfab.*, vol. 5, no. 3, 2006, Art. no. 033009.
[8] N. Vico Trivino, U. Dharanipathy, J.-F. Carlin, Z. Diao, R. Houdre, and N. Grandjean, "Integrated photonics on silicon with wide bandgap GaN semiconductor," *Appl. Phys. Lett.*, vol. 102, no. 8, 2013, Art. no. 081120.
[9] Y. Zhang *et al.*, "GaN directional couplers for integrated quantum photonics," *Appl. Phys. Lett.*, vol. 99, no. 16, 2011, Art. no. 161119.
[10] R. Hui *et al.*, "GaN-based waveguide devices for long-wavelength optical communications," *Appl. Phys. Lett.*, vol. 82, no. 9, pp. 1326–1328, 2003.
[11] K. Sasaki, N. Kawamura, H. Tokumaru, and Y. Sakane, "Waveguide of amorphous perfluoropolymer for visible light," *Appl. Phys. Lett.*, vol. 85, no. 7, pp. 1134–1136, 2004.
[12] Y. Q. Wang, J. Y. Shi, C. Yang, Y. G. Wang, and N. Chi, "Integrated 10 Gb/s multilevel multiband passive optical network and 500 Mb/s indoor visible light communication system based on Nyquist single carrier frequency domain equalization modulation," *Opt. Lett.*, vol. 39, no. 9, pp. 2576–2579, 2014.
[13] Z. Lai, Y. Wang, N. Allbritton, G.-P. Li, and M. Bachman, "Label-free biosensor by protein grating coupler on planar optical waveguides," *Opt. Lett.*, vol. 33, no. 15, pp. 1735–1737, 2008.
[14] B. Momeni, E. S. Hosseini, and A. Adibi, "Planar photonic crystal microspectrometers in silicon-nitride for the visible range," *Opt. Exp.*, vol. 17, no. 19, pp. 17060–17068, 2009.
[15] R. Dylewicz, R. A. Hogg, R. Airey, R. Paszkiewicz, P. Bientsman, and S. Patela, "Simulations of nanograting-assisted light coupling in GaN planar waveguide," *Opt. Quant. Electron.*, vol. 42, no. 9/10, pp. 619–629, 2011.
[16] D. Bai *et al.*, "Suspended GaN-based nanostructure for integrated optics," *Appl. Phys. B*, vol. 122, no. 1, p. 9, 2016.
[17] Q. Liu, Z. Shi, G. Zhu, W. Wang, Z. Wang, and Y. Wang, "Freestanding GaN grating couplers at visible wavelengths," *J. Opt.*, vol. 17, no. 4, 2015, Art. no. 045607.
[18] Z. Shi, X. Li, X. Fang, X. Huang, H. Zhu, and Y. Wang, "Experimental observation of lateral emission in freestanding GaN-based membrane devices," *Opt. Lett.*, vol. 39, no. 16, pp. 4931–4933, 2014.
[19] Y. Wang *et al.*, "Circular GaN membrane gratings," *IEEE Photon. Technol. Lett.*, vol. 26, no. 9, pp. 915–918, May 2014.
[20] Y. Wang, Z. Shi, X. Li, S. He, M. Zhang, and H. Zhu, "Surface-normal emission from subwavelength GaN membrane grating," *Opt. Exp.*, vol. 22, no. 1, pp. 667–672, 2014.
[21] D. Taillaert, W. Bogaerts, P. Dumon, D. Van Thourhout, and R. Baets, "Bridging the gap between nanophotonic waveguide circuits and single mode optical fibers using diffractive grating structures," *J. Nanosci. Nanotechnol.*, vol. 10, no. 3, pp. 1551–1562, 2010.
[22] A. Z. Subramanian, S. Selvaraja, P. Verheyen, A. Dhakal, K. Komorowska, and R. Baets, "Near-infrared grating couplers for silicon nitride photonic wires," *IEEE Photon. Technol. Lett.*, vol. 24, no. 19, pp. 1700–1703, Oct. 2012.
[23] Z. Xiao, T.-Y. Liow, J. Zhang, P. Shum, and F. Luan, "Bandwidth analysis of waveguide grating coupler," *Opt. Exp.*, vol. 21, no. 5, pp. 5688–5700, 2013.
[24] X. Zhao *et al.*, "Compact grating coupler for 700-nm silicon nitride strip waveguides," *J. Lightw. Technol.*, vol. 34, no. 4, pp. 1322–1327, 2016.

[25] M. Dai, L. Ma, Y. Xu, M. Lu, X. Liu, and Y. Chen, "Highly efficient and perfectly vertical chip-to fiber dual-layer grating coupler," *Opt. Exp.*, vol. 23, no. 2, pp. 1691–1698, 2015.
[26] C. J. Oton, "Long-working-distance grating coupler for integrated optical devices," *IEEE Photonics J.*, vol. 8, no. 1, Feb. 2016, Art. no. 2700208.
[27] H. Li *et al.*, "Investigation of the chip to photodetector coupler with subwavelength grating on SOI," *Opt. Laser Technol.*, vol. 76, pp. 79–84, 2016.
[28] G. Sharma, S. Kumar, and V. Singh, "Sensitivity of grating coupled graded thin film planar waveguide sensors," *Opt. Quant. Electron.*, vol. 47, no. 2, pp. 169–177, 2015.
[29] Q. Liu, Z. Gu, M. K. Park, and J. Chung, "Experimental demonstration of highly sensitive optical sensor based on grating-assisted light coupling between strip and slot waveguides," *Opt. Exp.*, vol. 24, no. 12, pp. 12549–12556, 2016.
[30] K. Hill, and G. Meltz, "Fiber Bragg grating technology fundamentals and overview," *J. Lightw. Technol.*, vol. 15, no. 8, pp. 1263–1276, 1997.
[31] D. Taillaert, P. Bienstman, and R. Baets, "Compact efficient broadband grating coupler for silicon-on-insulator waveguides," *Opt. Lett.*, vol. 29, no. 23, pp. 2749–2751, 2004.
[32] R. Halir *et al.*, "Recent advances in silicon waveguide devices using sub-wavelength gratings," *IEEE J. Sel. Topics Quantum*, vol. 20, no. 4, Jul./Aug. 2014, Art. no. 8201313.
[33] X. Chen, Z. Cheng, C. K. Y. Fung, and H. K. Tsang, "Design and applications of silicon waveguide grating couplers," *Proc. SPIE*, vol. 8266, 2012, Art. no. 82660I.
[34] Y. Wang, F. Hu, H. Sameshima, and K. Hane K, "Fabrication and characterization of freestanding circular GaN gratings," *Opt. Exp.*, vol. 18, no. 2, pp. 773–779, 2010.
[35] C. Hums, T. Finger, T. Hempel, J. Christen, A. Dadgar, A. Hoffmann, and A. Krost, "Fabry-Perot effects in InGaN/GaN heterostructures on Si-substrate," *J. Appl. Phys.*, vol. 101, no. 3, 2007, Art. no. 033113.